AIMS Energy, 9(4): 854–881.
DOI: 10.3934/energy.2021040
Received: 17 April 2021
Accepted: 21 June 2021
Published: 02 July 2021

http://www.aimspress.com/journal/energy

Research article

Solar energy storage in evacuated tubes solar collector using nanofluid embedded in a saturated porous media in the fully developed region: Al_2O_3 nanofluid embedded in graphite as a saturated porous media

Mohannad B. Khair[1,2,*] and Hamzeh M. Duwairi[1]

[1] Mechanical Engineering Department, School of Engineering, The University of Jordan, Amman, 11942 Jordan
[2] Graduate Student

* **Correspondence:** Email: khair.mohanad@gmail.com.

Abstract: The evacuated tube solar collector is considered an efficient, convenient, and economical option used to convert solar energy into heat. In this work, enhancement of evacuated tubes solar collector performance and the potential for energy storage by using Al_2O_3 water-based nanofluid embedded in Graphite as a saturated porous media was presented and studied theoretically. The Governing equations derived from the principles of conservation of mass, momentum, and energy were written in a dimensionless form, and solved these equations analytically for the fully developed region, and numerically throughout the entrance region, and the heat flux data for Amman, Jordan was used in this study. The analysis of the effect of different parameters as porosity, pore diameter, nanoparticles solid volume fraction, pressure, and radius of conduit on temperature variation through the pipe and Nusselt number was done. The results show that the flow of nanofluid in porous media enhances the evacuated tube's performance compared to just using water in the same medium under the same conditions. In August, the temperature variation in the evacuated tube at the same condition for Al_2O_3 water-based nanofluid for 1.5% volume fraction reach 42 ℃ and 73 ℃ for 6% volume fraction. In contrast, In January for the 1.5% volume fraction the temperature variation reached 25 ℃ and 43 ℃ for 6% volume fraction. On the other hand, the stored energy approximately reached 30 kJ/kg and 45 kJ/kg for solid volume fraction 1.5% and 6% respectively at the same conditions.

Keywords: solar energy; nanofluid; porous media; thermal storage; evacuated tube; solar collector

Abbreviations: Q: amount of heat stored, J; d_p: average particle or fiber diameter of the porous media, m; N: avogadro number; h: convective heat transfer coefficient, $W/(m^2.K)$; D: diameter of the conduit, m; z^*: dimensionless length; r^*: dimensionless radius of the conduit ; u^*: dimensionless velocity; k_{eff}: effective thermal conductivity of the porous medium, $W/(m.K)$; d_f: equivalent diameter of a base fluid molecule, m; d_{np}: equivalent diameter of solid nanoparticles, m; T_f: final temperature, ℃; p: fluid pressure, Pa; q'': heat flux per unit area, J/m^2; T_i: initial temperature, ℃; Nu_D: local nsselt number; m: Mass flow rate, kg/s; m: mass of heat storage medium, kg; Nu_m: mean nusselt number; M: molecular weight of the base fluid, kg/mol; Nu: nusselt number; R: outer radius of the conduit, m; P: perimeter of the tube, m; K: permeability of porous media, m^2; Pr: prandtl number; m^2; $\Delta P/L$: pressure gradient, Pa/m; Re_D: reynolds number based on darcy velocity; C_p: specific heat at constant pressure, $J/(kg.k)$; q: stored heat per unit mass, J/kg; T: temperature, ℃; T_e: temperature at the entrance, ℃; T_m: the mean temperature, ℃; v: the velocity at radial (r) direction, m/s; k: thermal conductivity, $W/(m.K)$; V_t: total volume of the porous medium, m^3; u_D: darcy velocity, m/s; u: velocity in z-direction, m/s; V_s: volume of the solid phase in the porous media, m^3; ρ: density, kg/m^3; ρ_{f0}: density of the base fluid at 293 K, kg/m^3; θ: dimensionless temperature; μ: dynamic viscosity, $Pa.s$; α_{eff}: effective thermal diffusivity, m^2/s; μ_{eff}: effective viscosity, $Pa.s$; $\emptyset$: nanofluid volume fraction; ε: porosity of porous media

1. Introduction

Renewable energy is considered an important source of clean energy. The negative impact of conventional energy sources on the environment and the fact that these resources will deplete, made most of the researches turn for the non-conventional renewable energy like solar, wind, geothermal, and hydropower.

Solar energy is the most available, environmentally friendly renewable energy source, a possible utilization by converting it to useful heat energy by using solar collectors. The evacuated tube solar collector is an efficient, convenient, and economical option for doing this [1].

The most straightforward, best promising technique for enhancing the performance of the evacuated tube solar collectors is using nanofluid as a working fluid, thus enhancing the thermal performance of the heat transfer fluid [2].

Nanofluids are an innovative, promising way to increase the heat transfer rate in the solar thermal collectors, by using them as working fluids instead of the conventional base fluids used before. Choi first proposed nanofluid in 1995 [3], Nanofluids formed by dispersing nano-solid particles from metal or metallic oxide into the base fluid, such as oil, water, and ethylene glycol. The nanofluids are engineered colloids made of solid nanoparticles with a size typically of 1–100 nm, which are suspended in liquids [4].

The use of proper techniques for heat transfer enhancement is vital to optimizing energy devices, and nanofluid utilization is one of the relatively new solutions to accommodate this purpose. Since nanofluids have high thermal conductivity compared to the base fluids used before, they can improve the heat transfer rate in solar thermal collectors as one of the engineering systems that may be used with it. Currently, nanofluid is a hot topic, and many researchers around the world are working on it [5].

From the need to store the solar energy during its availability and reuse it at the time of requirement and maximize the efficiency of the energy conversion from solar to thermal energy, porous materials were widely used in solar systems, because it can improve the heat transfer characteristics in

solar systems by offering a high ratio of surface area to volume. It can act as an energy storage medium since it represents a packed bed storage system at a macroscopic level [6].

An attractive technique to enhance the heat transfer is the usage of porous media, such as the application of metal-based porous materials such as copper foams in channels and heat exchangers. Porous media consists of a solid matrix containing pores (voids), which are typically filled with fluid. Porous media are rigid, open-cell, and saturated, which means that the pores are connected and filled with the fluid completely so that the fluid can flow through the voids. Recently, the technique of using both nanofluid and porous media has received considerable attention and has led to extensive investigations in this field [7].

Porous media has the potential to increase the contact surface area between the fluid and solid surface. On the other hand, nanoparticles dispersed in nanofluid enhance the effective thermal conductivity. Therefore, it seems that using both porous media and nanofluid can augment the efficiency of typical thermal systems dramatically [5].

One of the techniques to enhance the convective heat transfer is to employ solid materials, such as nanoparticles or porous media, with higher thermal conductivity concerning the traditional base fluids. The usage of such materials also allows a significant increase of heat transfer contact area inside the fluids, and the heat transfer passes from a surface exchange to a bulk or mass exchange. The coupling of nanoparticles and porous media with high thermal conductivity is an interesting and promising solution. Many research activities have been developed in the convective heat transfer of nanofluids in porous media [8].

Muhammad [9] reviewed different models to enhance the thermal performance of flat plate and evacuated tube solar collectors by using nanofluids.

Gautam and Saini [6] considered the packed bed as a porous media at the macroscopic level, and they did a review on technical, applications, and economic aspects of packed bed solar thermal energy storage systems. The description of the packed bed storage system and its working principle and design aspects were discussed. Various factors affecting the heat transfer involved within a packed bed were described. The packed bed storage system (PBSS) has three major components, which are the storage medium, energy transfer mechanism, and contaminated systems. The storage medium keeps the sensible heat inside it in the form of sensible heat, latent heat, or thermo-chemical form. The energy transfer mechanism used to extract or supply energy to the storage medium by the flow of the heat transfer fluid. The job for the contaminated system is to hold storage medium, energy transfer mechanism, and different accessories needed for the PBSS.

Rashidi [10] reviewed the applications of porous materials in solar systems, their advantages, and their limitations. Different energy conversion and storage systems that use porous materials were presented. It was concluded that the use of porous media inside a solar system is considered as an easy and simple modification that can enhance and improve the efficiency of that system. The effect of the porous media is positive for heat transfer. In comparison, the opposite happens with the pressure drop. Thus, it required more pumping power.

Ahmed and Mohammed [11] studied the performance of the double pass PV/thermal collector air collector. They concluded that the heat transfer area is increased due to the use of the porous medium. Thus, it reflects directly to increase in the temperature of the exit air from the hybrid PV/thermal collector and the thermal efficiency of the system was increased with the presence of the porous media almost 29%.

Saryazdi [4] studied numerically the forced convection flow and heat transfer of nanofluid

flowing inside a straight circular pipe filled with a saturated porous medium, the finite volume method used to analyze the heat transfer coefficient of Al_2O_3-water nanofluid. It is approved that the local Nusselt number is increased with the increase of the nanoparticles volume fraction. Still, the increase is not significant and almost not clearly observed. That is due to the effective thermal conductivity of porous media that has great value, and this originally comes from the high thermal conductivity of the porous media material used.

Tajik Jamal-Abad [12] experimented with the effect of partially metal foam inside the absorber of parabolic trough solar collectors. The copper foam was used, and the results showed that the absorber filled with metal foam enhanced and improved the efficiency because the enhancement happens in the thermal conductivity.

AlMasa'deh and Duwairi [13] modeled analytically and numerically the fluid flow and heat transfer inside a saturated porous conduit at constant surface heat flux. The energy, momentum, and continuity equations were solved by using a theoretical model with constant heat flux boundary conditions through the fully developed and entrance region. The results indicate that the porous media has very good potential to enhance the heat transfer rate.

Saedodin [14] carried out experimental and numerical investigations on the performance of a flat plate solar collector filled with porous copper metal foam. The numerical and experimental results showed that the use of porous media enhances the flat plate solar collector's performance, where the Nusselt number and the maximum thermal efficiency are enhanced by 82% and 18.5%, respectively.

Esfe [15] reviewed the heat transfer of nanofluids in porous media for different nanofluids and porous media in a forced, natural, and mixed convection systems. It is found that porous media can improve the performance and heat transfer in various applications. While the nanofluids considerably enhance the thermal conductivity of the working fluid. Consequently, using both porous media and nanofluids can significantly improve the thermal efficiency in the thermal systems.

Alihosseini and Jafari [16] studied the effect of porous medium configuration on nanofluid heat transfer using the computational fluid dynamics model. Al_2O_3 water-based nanofluid was used as a working heat transfer fluid with aluminum foam as a porous medium. Different configurations were used and compared with each regarding the enhancement parameter and the Nusselt number. It was concluded that, the fully saturated porous cylinder gave the best results among the other configurations.

Esmaeili [17] investigated numerically the performance of a direct absorption solar collector using CuO water-based nanofluid and copper oxide porous foam by using the finite volume technique to solve the mathematical model suggested. The best performance and efficiency obtained when the collector was fully filled with porous metal oxide foam. Moreover, the results proved that using nanofluid and porous media enhances efficiency by 26.8% compared to the flow of water without porous media.

Tay [18] reviewed different techniques for phase change material that moved in the thermal energy storage systems. The results showed that the use of transporting phase change material gave an efficient economic low cost heat transfer and a high compactness factor for the thermal energy storage. Another work was done by Liu [19] were they reviewed several models to enhance the thermal conductivity of phase change material for thermal energy storage. Where the importance of enhance the conductivity of the phase change material is essential due to reach a high energy charging/discharging rates.

The enhancement of the finned heat pipe performance using nano-enhanced H_2O as phase change material was studied by Lohrasbi [20], the study was based on a latent heat thermal energy storage

system in a finned heat pipe impeded into the nano-enhanced phase change material. The results were obtained numerically and showed that it can be achieve the efficient design of the latent heat thermal energy storage system by using the maximum energy storage capacity as an evaluation parameter.

Another model for energy storage was studied by Bazri [21], the latent heat storage tank was used in combination with a solar heater system using evacuated heat pipe solar collectors connected to a tank full with paraffin was as a phase change material. The results showed that there is a promising enhancement in the efficiency and reached to 58% compared to the baseline.

Naghavi [22] studied an on-demand dynamic performance of a thermal battery in tankless domestic solar water heating, that done by collecting and storing the solar energy in a latent heat storage tank that used as a thermal battery, this solar heat used in a heat exchanger to provide a hot water for the domestic use. The results showed a promising results with a 2 m^2 solar collector size that proved it can provide at least 112 liters per day in the worst weather condition.

2. Mathematical modeling

This study deal with the forced convection problem inside a saturated porous media with a constant surface heat flux, the Darcy model is taken for this case.

A theoretical model for nanofluid flow in a saturated porous media was build and solved analytically, with studying the effect of some factors (porosity, pressure.etc) on the temperature variation to illustrate the difference of using water and nanofluid in energy storage. The study shows the energy storage in August (summer) and January (winter) in Amman city.

For understanding the nanofluid thermophysical properties, the nanofluid volume fraction should be defined. The nanofluid volume fraction (∅) is the constituent volume divided by all constituent volumes of the mixture before mixing, as shown in Eq 1. It is found that increasing the nanoparticles volume fraction increases thermal conductivity [23].

$$\emptyset = \frac{V_{np}}{V_{total}} \tag{1}$$

A weighted average process with the volume concentration between the nanoparticles and the base fluid is accomplished to find the nanofluid's thermal properties. For the density, a simple mass balance is applied, as shown in Eq 2.

$$\rho_{nf} = \emptyset\rho_{np} + (1 - \emptyset)\rho_f \tag{2}$$

For the specific heat, the simple weighted average with the concentration as in Eq 3 will not give an accurate result.

$$C_{p_{nf}} = \emptyset\left(C_p\right)_{np} + (1 - \emptyset)\left(C_p\right)_f \tag{3}$$

It is better to use an analytical model by assuming thermal equilibrium between nanoparticles and the base fluid as in Eq 4 [24].

$$C_{p_{nf}} = \frac{\emptyset\left(\rho C_p\right)_{np} + (1-\emptyset)\left(\rho C_p\right)_f}{\rho_{nf}} \tag{4}$$

The Corcione Eq [25] will be used in this work to simulate the dynamic viscosity

$$\mu_{nf} = \mu_f \frac{1}{1 - 34.87(\frac{d_{np}}{d_f})^{-0.3} \emptyset^{1.03}}$$

where d_f is the equivalent diameter of a base fluid molecule, given by

$$d_f = 0.1 \left(\frac{6M}{N\pi\rho_{f0}}\right)^{1/3} \quad (5)$$

In which M is the molecular weight of the base fluid, N is the Avogadro number, and ρ_{f0} is the density of the base fluid calculated at temperature $T_0 = 293\ K$.

For this work, Aluminum Oxide nanoparticles (Al_2O_3) with water as a base fluid were used as the working heat transfer fluid. The thermophysical properties of the Al_2O_3 and water are given in Table 1 [26].

Table 1. Thermo-physical properties of the water and Al_2O_3.

	ρ (kg/m^3)	Cp (J/kg K)	k (W/m K)	d_{np} (nm)
Pure water	997.1	4179	0.613	-
Al_2O_3	3970	765	40	25

The properties of Graphite were used in calculations of this study are shown in Table 2 [27,28].

If total volume of the media, and the solid volume are known, literally porosity could be defined as follow.

$$\varepsilon = 1 - \frac{V_s}{V_t} \quad (6)$$

where ε is the porosity of the medium, V_s and V_t are respectively the volume of the solid phase and total volume of the medium.

Table 2. Properties of graphite are used in analytical calculation.

Thermal conductivity (W/m K)	25–470
Heat capacity (J/g K)	0.7
Average particles or pore diameter (mm)	350
Density (kg/m^3)	2260

Permeability is a geometrical characteristic of the porous media. It is important because it has a direct effect on the directional movement and the flow rate of the working fluids. For particle beds and fibers, permeability can be defined utilizing the Carman-Kozeny theory as follows [7,29].

$$K = \frac{\varepsilon^2 {d_p}^2}{150(1-\varepsilon)^2} \quad (7)$$

where d_p is the average particle or fiber diameter.

Graphite has an important advantage that it does not react with any of the organic material. Thus,

it considered having chemically inert characteristics at the room temperature. Graphite is being used in various applications such as electrical transfer devices, thermal transfer devices, and electrochemical super capacitors. Graphite is well known for the high thermal conductivity that it has. Thus, it gave it the capability to serve as a good porous media, where the high thermal conductivity will lead to enhance the heat transfer rate [30,31].

The Darcy velocity of the nanofluid (u_D) is given by the following Eq,

$$u_D = \frac{K}{\mu_{eff}} \frac{\Delta P}{L} \tag{8}$$

where μ_{eff} is the effective viscosity, μ is the nanofluid viscosity and K is the permeability of the porous media. The Einstein's formula for dilute suspensions can be used [32].

$$\mu_{eff} = \mu_{nf}[1 + 2.5(1 - \varepsilon)] \tag{9}$$

Reynold number can be calculated for nanofluid based on pores diameter or based on permeability. The studies found that calculating Reynolds number based on pore diameter is more accurate since permeability and inertial resistance are dependent on pore size [23].

Reynolds number based on pores diameter can be found using the below Eq.

$$Re_D = \frac{\rho_{nf}\, u d_p}{\mu_{nf}} \tag{10}$$

And Reynolds number based on permeability is:

$$Re_K = \frac{\rho_{nf} u \sqrt{K}}{\mu_{nf}} \tag{11}$$

The suggested model examines enhancement of the performance of evacuated tube by nanofluid flowing in a saturated porous media, the tube is taken to be evacuated to restrict convective and conductive heat losses to the ambient. The governing equations were written and solved in the two-dimensional system (r, z). The continuity, momentum, and energy Eqs were solved simultaneously for intention to Darcy effects on fluid flow and heat transfer inside a saturated porous conduit.

As a governing principle in fluids, the fluid flow is controlled and governed by the conservation laws of momentum, energy and mass.

In the present study, the suggested model was developed using the above conservation equations. Taking into consideration that the momentum equations for fluid flow with the presence of porous media differ from the absence of it.

A two-dimensional forced convection incompressible nanofluid flow in a circular tube saturated with porous media, as illustrated in Figure 1.

For the mathematical model in this study, the following assumptions were taken:

1. The nanofluid flow is steady, incompressible, laminar, forced fluid flow in two-dimensions.
2. The temperature of the nanofluid is below the boiling point.
3. The nanofluid and solid matrix are everywhere in thermodynamics equilibrium.
4. All the physical properties of the fluid are isotropic and homogeneous

The dimensional governing equations that describe the convection flow can be written as follows:

- The continuity Eq (the conservation of mass)

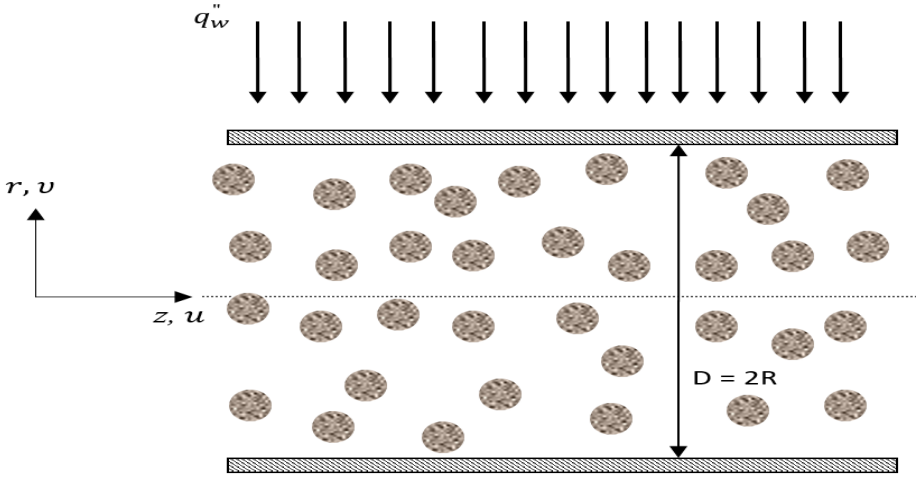

Figure 1. Physical model and coordinate system.

The continuity equation is based on the principle of conservation of mass, since the total mass flow in will equal the total mass flow out from a specified control volume if there is no mass storage or loss in the system.

$$\frac{1}{r}\frac{\partial(vr)}{\partial r}+\frac{\partial u}{\partial z}=0 \tag{12}$$

- The z-momentum Eq (conservation of momentum):

Since the velocity is pure Darcy velocity, the below equation can be written:

$$u=u_D=\frac{-K}{\mu}\frac{\partial p}{\partial z} \tag{13}$$

- The r-momentum Eq (conservation of momentum):

$$v=\frac{-K}{\mu}\frac{\partial p}{\partial r} \tag{14}$$

- The energy Eq (conservation of energy):

$$u\frac{\partial T}{\partial z}+v\frac{\partial T}{\partial r}=\alpha_{eff}\left(\frac{\partial^2 T}{\partial z^2}+\frac{\partial^2 T}{\partial r^2}+\frac{1}{r}\frac{\partial(T)}{\partial r}\right) \tag{15}$$

where K, p, μ, T, and α_{eff} is permeability, fluid pressure, dynamic viscosity, fluid temperature, and the effective thermal diffusivity (m^2/s) respectively.

where α_{eff} can be calculated using the following Eq:

$$\alpha_{eff}=\frac{k_{eff}}{(\rho C_p)_{nf}} \tag{16}$$

where

$$k_{eff}=\varepsilon k_{nf}+(1-\varepsilon)k_s \tag{17}$$

Is the effective thermal conductivity of the porous medium. k_{nf} and k_s are the thermal conductivity of the nanofluid, and the solid porous media respectively, and ε is porosity of the porous media.

The governing boundary conditions for the model suggested is:

- The velocity in the $r\text{-}direction$ can be neglected ($\upsilon = 0$).
- The heat transfer in the r direction at the center of the pipe is equal to zero ($\partial T/\partial r = 0\ at\ r = 0$).

Thus, the boundary conditions above were used in this work as the following formula

- At the outer surface:

$$\text{At}\quad r = R \qquad \rightarrow \qquad q_w^{"} = +k\frac{\partial T}{\partial r} = h(T_w - T_c)$$

- At the center:

$$\text{At}\quad r = 0 \qquad \rightarrow \frac{\partial T}{\partial r} = 0$$

Since the velocity in the $r\text{-}direction$ was neglected ($\upsilon = 0$), and there is no heat transfer in the radial direction at the center ($\partial T/\partial r = 0\ at\ r = 0$). The heat diffused in the z-direction were neglected compared to the heat diffused in the radial direction (r).

Energy Eq can be reduced to:

$$u\frac{\partial T}{\partial z} = \alpha_{eff}\left(\frac{\partial^2 T}{\partial z^2} + \frac{\partial^2 T}{\partial r^2} + \frac{1}{r}\frac{\partial T}{\partial r}\right) \tag{18}$$

The initial point of the conduit has no heat transfer so the temperature is uniform and constant and can be presented as $= T_e$, at $z = 0$.

In the fully developed region, the relative shape of the temperature profile remains the same but T_m always vary in the Z-direction i.e., $\frac{\partial T_m}{\partial Z} \neq 0$.

The temperature profile in the fully developed region can be found by the following Eq [33].

$$\frac{\partial}{\partial z}\left[\frac{T_w(z) - T(z)}{T_w(z) - T_c(z)}\right] = 0 \tag{19}$$

The conduction heat transfer rate in the axial direction along the pipe will be negligible compared to the one that is in the radial direction, so $\frac{\partial^2 T}{\partial z^2}$ was ignored compared to $\frac{\partial^2 T}{\partial r^2}$ [33].

Thus, the energy Eq becomes:

$$u\frac{\partial T}{\partial z} = \alpha_{eff}\left(\frac{\partial^2 T}{\partial r^2} + \frac{1}{r}\frac{\partial T}{\partial r}\right) \tag{20}$$

By arranging Eq 19 and substitute it into Eq 20, the energy Eq becomes

$$u\frac{dT_w}{dz} = \alpha_{eff}\left(\frac{\partial^2 T}{\partial r^2} + \frac{1}{r}\frac{\partial T}{\partial r}\right) \tag{21}$$

Substitute temperature profile and Darcy velocity into energy Eq:

$$\left(\frac{-K}{\mu}\frac{\partial p}{\partial z}\right)\frac{dT_w}{dz} = \alpha_{eff}\left(\frac{\partial^2 T}{\partial r^2} + \frac{1}{r}\frac{\partial T}{\partial r}\right) \tag{22}$$

The left term of the above Eq is a constant, the symbol C^* will be used instead of the left term in Eq 22 to simplify the solution.

By substitute the left term in Eq 22 by C^* and multiplying the Eq by (r):

$$r(\times \frac{C^*}{\alpha_{eff}} = r \times (\frac{\partial^2 T}{\partial r^2} + \frac{\partial T}{\partial r})$$

$$r\frac{C^*}{\alpha_{eff}} = \frac{\partial}{\partial r}\left(r\frac{\partial T}{\partial r}\right) \tag{23}$$

By integrating Eq 23 twice and applying the boundary conditions and because the model is subjected by constant heat flux we get

$$T = T_w + \frac{q''}{2\,R\,k}(r^2 - R^2) \tag{24}$$

Now to find Nusselt number we should find mean temperature T_m to substitute it in the heat transfer coefficient. So, from Newton's Law of Cooling heat transfer coefficient is:

$$h = \frac{q''}{T_w - T_m} \tag{25}$$

The mean temperature T_m can be found as the following [33]:

$$T_m = \frac{2}{u_m R^2}\int_0^R uT\,r\,dr \tag{26}$$

Substitution Eq 24 into Eq 26 and the result is integrated over the interval $[0, R]$. Finally, mean temperature represented as follows:

$$T_m = T_w - \frac{q''}{4k}\,R \tag{27}$$

Substitute Eq 27 into 25 to get:

$$h = \frac{4k}{R} \tag{28}$$

Now the Nusselt number is founded by substitute the heat transfer coefficient found in Eq 28 in Nusselt number Eq $\left(\frac{hD}{k}\right)$, where $D = 2R$. Since the heat flux concentrated on a one half of the tube, the Nusselt number will be as:

$$Nu = 4$$

3. Solutions validation

In the entrance region or developing region where the boundary layer develops and reaches the tube center, the developing in velocity profile is then essentially fully developed before the heat transfer take place, and because of the presence of porous media, the velocity profile is not changing with z along the conduit which means there is only a thermal entrance region. The following

dimensionless variables are used in case of constant heat flux at the wall:

$$\theta = \frac{T - T_e}{q'' D/k} \qquad u^* = \frac{u}{u_D}$$

$$r^* = \frac{r}{D} \qquad z^* = \frac{z}{D} \tag{29}$$

where θ is the dimensionless temperature, T_e is the temperature at the entrance point, u^* is dimensionless velocity, u_D is the Darcy velocity in the conduit, D is the diameter of the conduit ($D = 2R$), z^* is the dimensionless length and r^* is the dimensionless radius of the conduit.

By substituting dimensionless variables in the energy Eq, the energy Eq will be as the following after substitute the effective thermal diffusivity:

$$u^* \frac{\partial \theta^*}{\partial z^*} = \frac{1}{Pr\ Re}\left(\frac{\partial^2 \theta^*}{\partial r^{*2}} + \frac{1}{r^*}\frac{\partial \theta^*}{\partial r^*}\right) \tag{30}$$

The dimensionless velocity u^* can be eliminated, since the velocity through porous media is constant and here is Darcy velocity which means $u = u_D$ so $u^* = 1$.

The following is the dimensionless boundary conditions for the above Eq.

The initial condition:

$$\theta = 0 \quad as \qquad z^* = 0$$

The boundary conditions

$$\frac{\partial \theta}{\partial r^*} = 0 \quad as \quad r^* = 0\ and$$

$$\frac{\partial \theta}{\partial r^*} = 1 \qquad as \qquad r^* = 0.5 \tag{31}$$

The linear second-order differential Eq 30 concerning boundary conditions Eq 31 was solved by finite difference method using MATLAB program.

Thus, using the FDM approach we get the following Eq:

$$\frac{\theta(z^*,r^*) - \theta(z^* - \Delta z^*, r^*)}{\Delta z^*} = \frac{1}{Pr\ Re}\left(\frac{\theta(z^*,r^* + \Delta r^*) - 2\theta(z^*,r^*) + \theta(z^*,r^* - \Delta r^*)}{\Delta r^{*2}} + \frac{1}{r}\frac{\theta(z^*,r^*) - \theta(z^*,r^* - \Delta r^*)}{\Delta r^*}\right) \tag{32}$$

We can write the dimensionless temperature at constant heat flux at the wall as:

$$\theta|_{r^*=0.5} = \frac{T_w - T_e}{q'' D/k} \tag{33}$$

So, we can calculate local Nusselt number by the following formula.

$$Nu_D = \frac{1}{\theta|_{r^*=0.5}} \tag{34}$$

where Nu_D is the local Nusselt number.

The Nusselt number is defined in terms of the difference between the wall and the mean temperatures ($T_w - T_m$).

The mean temperature T_m can be found as the following [33]:

$$T_m = \frac{2}{u_m R^2} \int_0^R uT\, r\, dr \tag{35}$$

Temperature T can be obtained from dimensionless form Eq 31:

$$T = \theta \left(\frac{q'' D}{k}\right) + T_e \tag{36}$$

Substitution Eq 34 into Eq 33 and $u = u_m$ we get:

$$\frac{T_m - T_e}{q'' D/k} = \frac{2}{R^2} \int_0^R \theta\, r\, dr \tag{37}$$

A right side represent a non-dimensional mean temperature θ_m.
After substituting the dimensionless form from Eq 31 the result will be:

$$\theta_m = 8 \int_0^{r^*} \theta\, r^*\, dr^* \tag{38}$$

Equation 38 was solved using MATLAB, and the results used to find the Nusselt number using the following Eq.

$$Nu_{D\,m} = \frac{1}{2(\theta_w - \theta_m)} \tag{39}$$

Figures 2 and 3 show the results of these Eqs.

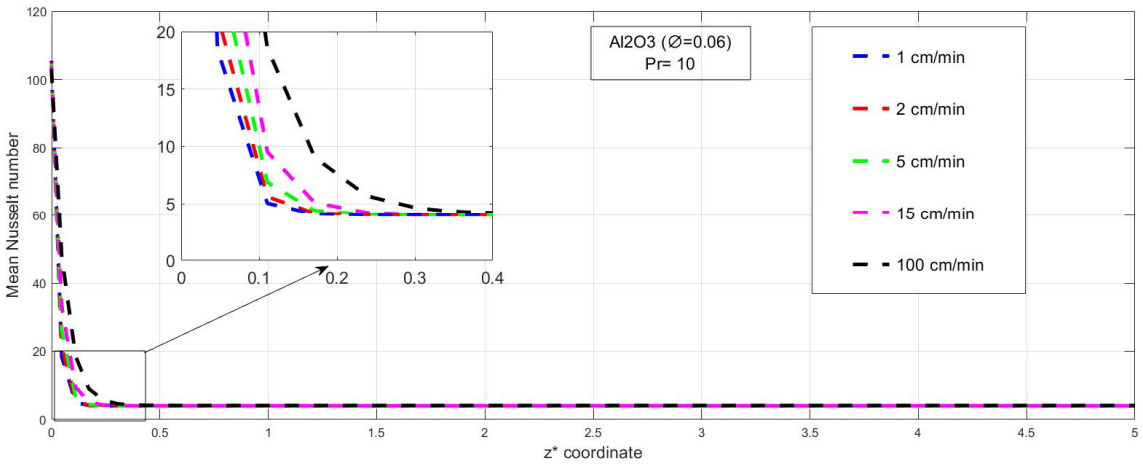

Figure 2. Mean Nusselt number along the conduit at different velocities for Al_2O_3 nanofluid.

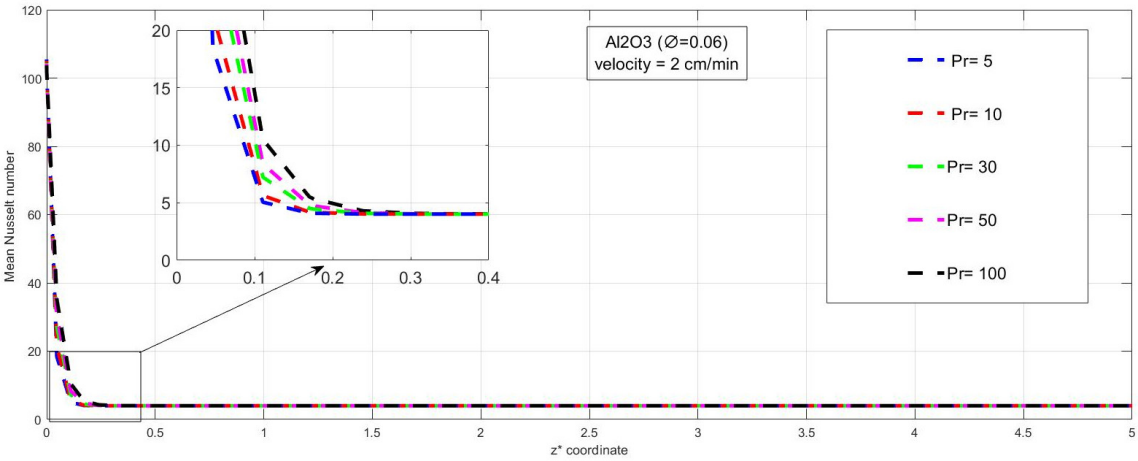

Figure 3. Mean Nusselt number along the conduit at different Prandtl number for Al_2O_3 nanofluid.

The enhancement of the convection heat transfer relative to the conduction through the same fluid layer is expressed by the Nusselt number. Where the higher the Nusselt number is, the more the convection heat transfer is effective.

The Nusselt number shows the enhancement of heat transfer through a fluid boundary as a result of convection relative to conduction across the same fluid layer. The larger the Nusselt number, the more effective the convection.

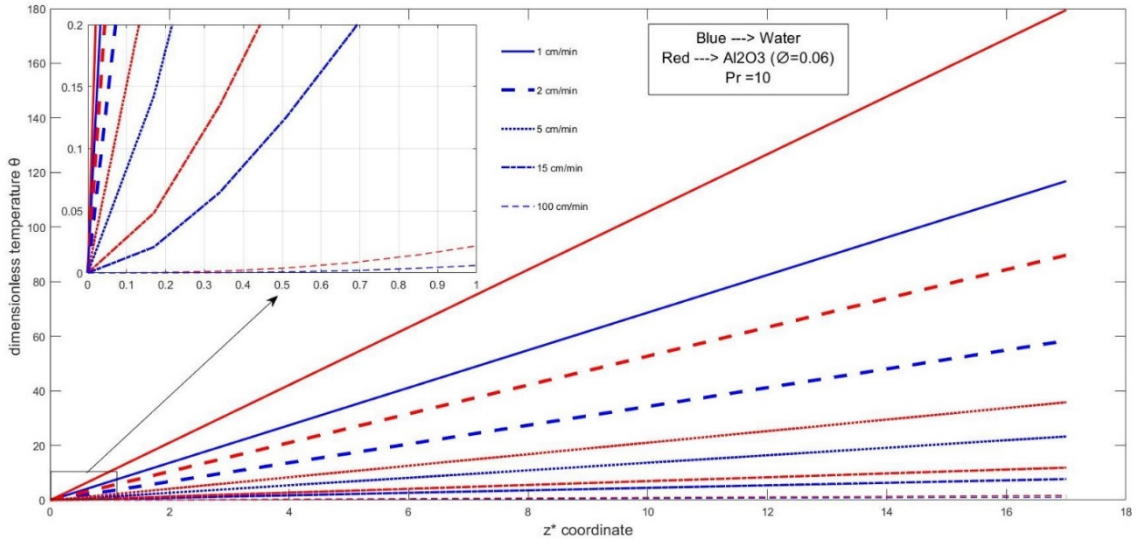

Figure 4. Dimensionless temperature θ at different axial coordinate z* at different velocities for water and Al_2O_3 nanofluid.

In the entrance region, the mean Nusselt number was found and it can be presented in an exponential distribution. The Nusselt number starts with a high value then dramatically decrease to reach the fully developed region. In the fully developed region, the Nusselt number that was found analytically remains constant. Obviously, the Nusselt number in the entrance region is decreased to

reach the value of the fully developed region. The value of Δz and Δr in the numerical solution is the largest value when does not change the solution in order to the staked solution.

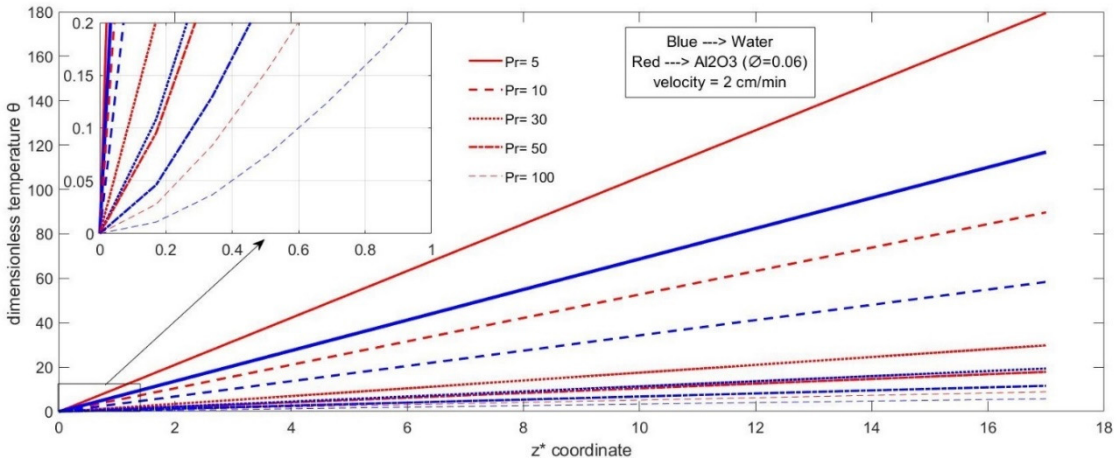

Figure 5. Dimensionless temperature θ at different axial coordinate z* at different Prandtl number for water and Al_2O_3 nanofluid.

Figures 4 and 5 present the dimensionless temperature θ with axial coordinate z* at different fluid velocities and Prandtl numbers (Pr) respectively for water and Al_2O_3 water-based nanofluid. It is noted that the temperature increases in the axial direction of the flow, thus because the continuous heating of the fluid in the entrance region. From the mentioned figures before, it is concluded that the increase in the fluid velocity and Prandtl number cause to decrease in temperature profile and this because of increasing in the fluid velocities means increasing in Reynolds numbers and thus increasing in inertia forces and increasing in heat transfer coefficient. Also, the increase in Prandtl number caused a decrease in fluid temperatures, that enhance heat transfer rates. In the same conditions, nanofluid reach higher dimensionless temperature than water did, and especially when the fluid velocities were low the dimensionless temperature difference was higher.

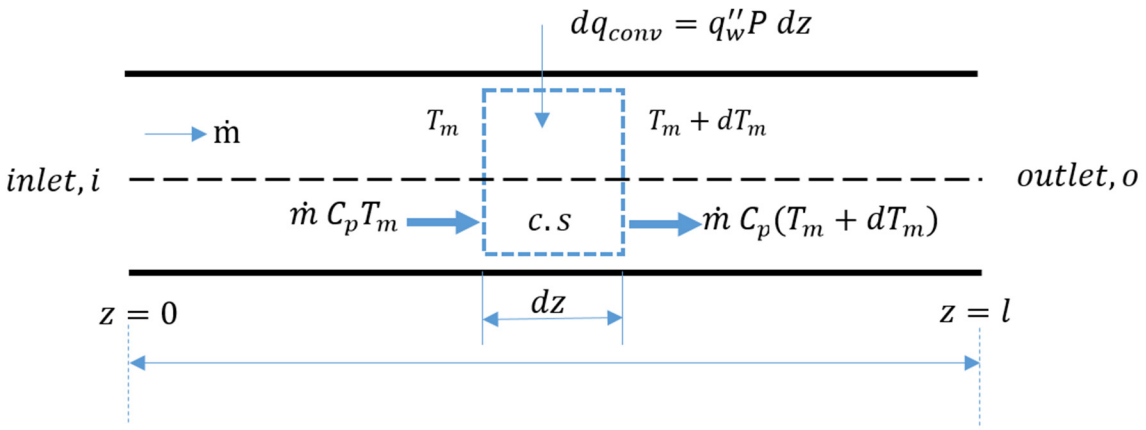

Figure 6. Energy and mass balance through conduit.

Along the pipe, the temperature is varied in the z-direction. The mean temperature variation in the axial direction can be calculated by applying the energy balance Eq as presented in Figure 6.

A differential control volume is taken, and the energy conservation is applied at constant heat flux surface, that leads for the following:

$$\frac{dT_m}{dz} = \frac{q''_w P}{\dot{m}\, c_p} \tag{40}$$

where P is the perimeter of the tube, and $\mathrm{c_p}$ is the specific heat.

Since the temperature gradient is independent of the axial position in the fully developed flow, the shape of the temperature profile will be the same without any change along the tube in that region.

By Integration of Eq 40 at ($T_m = T_{m_i}$ as $\mathrm{z} = 0$) and substituting into it $\mathrm{P} = 2\pi\mathrm{R}$, and $\dot{\mathrm{m}} = \rho \mathrm{u_m} \mathrm{A_c} = \rho \mathrm{u_m} \pi \mathrm{R}^2$ leads to:

$$T_m = \frac{2q''_w}{(\rho c_p)_{eff} u_m R} + T_{m_i} \tag{41}$$

where

$$(\rho c_p)_{eff} = \varepsilon(\rho c_p)_{nf} + (1-\varepsilon)(\rho c_p)_s \tag{42}$$

Is the heat capacity per unit volume and $\mathrm{u_m}$ is the mean velocity of the fluid which is equivalent to the Darcy velocity.

Heat flux at the wall in Eq 41 is the irradiance (W/m^2), the irradiance for Amman city in Jordan was taken in our work, and the data of the irradiance were taken from "Photovoltaic Geographical Information System" (PVGIS). The data for Amman irradiance is given in Table 3.

The stored energy can be calculated by using the following Eq.

$$Q = \int_{T_i}^{T_f} m\, C_p\, dT = m\, C_p\, (T_f - T_i) = m\, C_p\, \Delta T \tag{43}$$

The sensible heat storage for the material depends on its heat capacity which is the energy density, and the thermal diffusivity which is the rate that the heat extracted and released.

Where Q is the amount of heat stored, T_i and T_f are respectively, the initial temperature, and the final temperature, m is the mass of heat storage medium, and $\mathrm{C_p}$ is the specific heat.

The stored energy per unit of mass can be calculated using the following Eq.

$$\frac{Q}{m} = \mathrm{q} = C_p\, \Delta T \tag{44}$$

Table 3. Irradiance data for Amman. **From JRC Photovoltaic Geographical Information System (PVGIS).

Time (hour）	Month											
	Jan	Feb	Mar	Apr	May	Jun	Jul	Aug	Sep	Oct	Nov	Dec
5	0	0	0	0	0	0	0	0	0	0	0	0
6	0	0	5.12	20.77	38.7	55.42	45.92	34.1	32.63	15.87	0.04	0
7	41.56	51.47	92.5	130.71	179.5	219.23	213.7	195.69	191.11	167.3	113.67	66.21
8	175.83	178.93	245.29	295.9	352.95	420.84	414.36	396.95	399.63	358.03	279.59	219.62
9	315.54	318.47	405.65	477.34	519.7	592.1	596.66	589.21	596.79	535.94	440.39	357.06
10	431.58	435.37	542.23	601.52	650.64	730.05	733.83	736.3	737.72	660.28	517.48	474.67
11	485.98	509.91	603.29	669.99	706.8	758.03	814.76	818.19	805.38	715.28	560.88	520.97
12	485.71	516.23	608.75	677.95	708.72	808.7	821.81	825.98	804.31	715.79	576.95	498.86
13	435	470.95	574.22	620.6	669.94	747.64	762.42	765.26	704.74	618.68	495.33	440.45
14	321.76	362.39	458.05	499.04	540.38	617.7	643.16	630.5	505.29	384.95	344.23	306.76
15	198.71	237.23	319.87	353.13	371.14	450.3	469.56	455.88	381.99	278.13	170.96	170.01
16	59.63	91	156.07	182.88	202.44	264.33	282.3	260.5	202.21	90.57	37.51	19.28
17	0	4	25.21	38.68	51.73	84.69	97.69	78.55	26.61	0	0	0
18	0	0	0	0	0	0	0	0	0	0	0	0

**https://ec.europa.eu/jrc/en/pvgis

4. Results and discussions

The enhancement of the convection heat transfer relative to the conduction through the same fluid layer is expressed by the Nusselt number. Where the higher the Nusselt number is, the more the convection heat transfer is effective.

The Nusselt number shows the enhancement of heat transfer through a fluid boundary as a result of convection relative to conduction across the same fluid layer. The larger the Nusselt number, the more effective the convection.

The local Nusselt number at different nanofluid velocities and Prandtl numbers were illustrated respectively, in Figures 7 and 8. The local Nusselt number was found by taking the difference between the outer surface and the entrance temperatures. The local Nusselt number profile was facing a sharp decrease until it hit the zero, that is because of the temperature difference decrease between the outer surface temperature and the entrance temperature along the tube. It is noted that the higher the nanofluid velocities and Prandtl numbers are, the longer the entrance region length is, and that is unpreferable. For that reason, it is recommended for the better performance to keep the nanofluid velocity and the Prandtl numbers as low as possible.

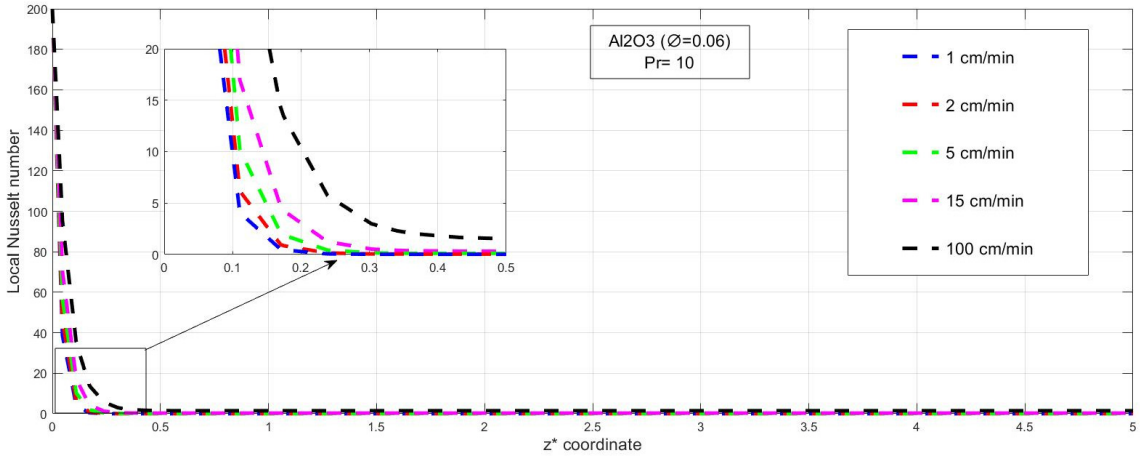

Figure 7. Local Nusselt number along the conduit at different velocities for Al_2O_3 nanofluid.

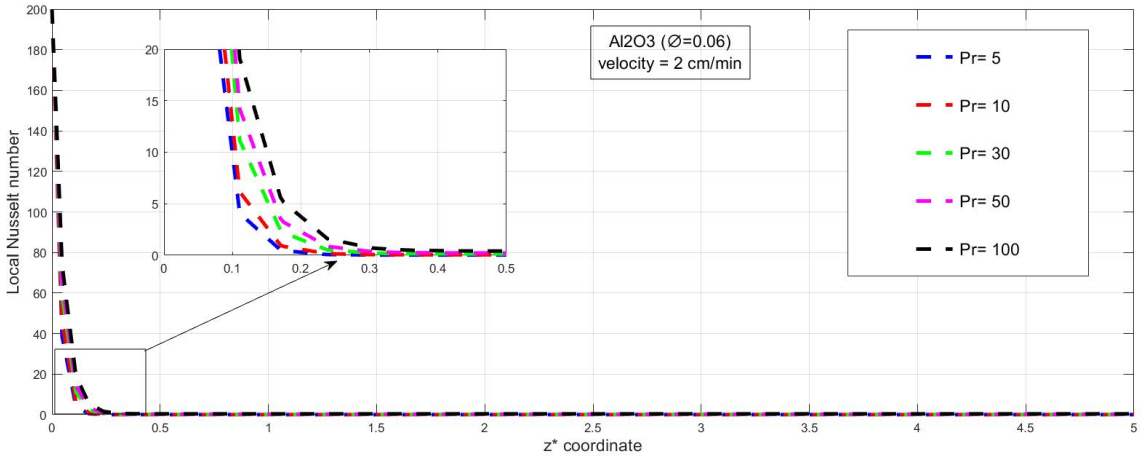

Figure 8. Local Nusselt number along the conduit at different Prandtl number for Al_2O_3 nanofluid.

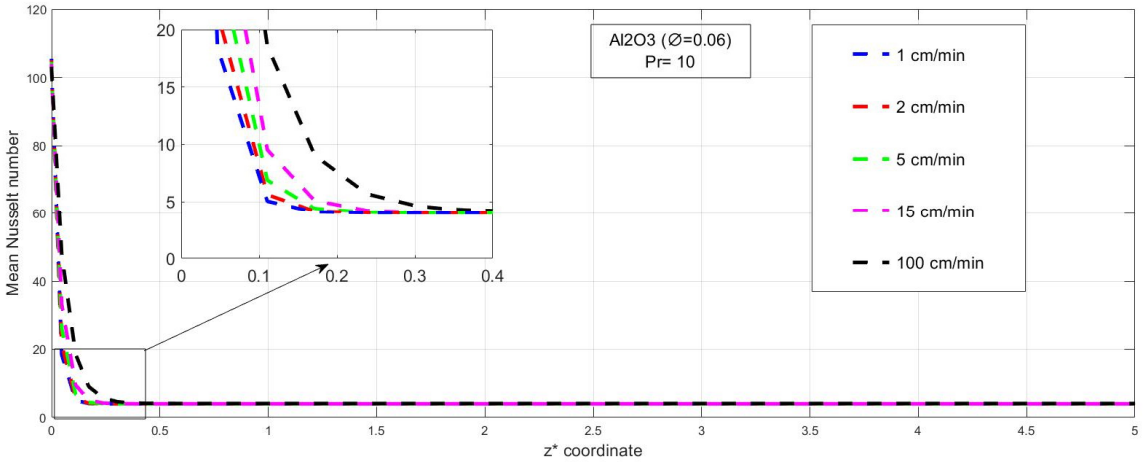

Figure 9. Mean Nusselt number along the conduit at different velocities for Al_2O_3 nanofluid.

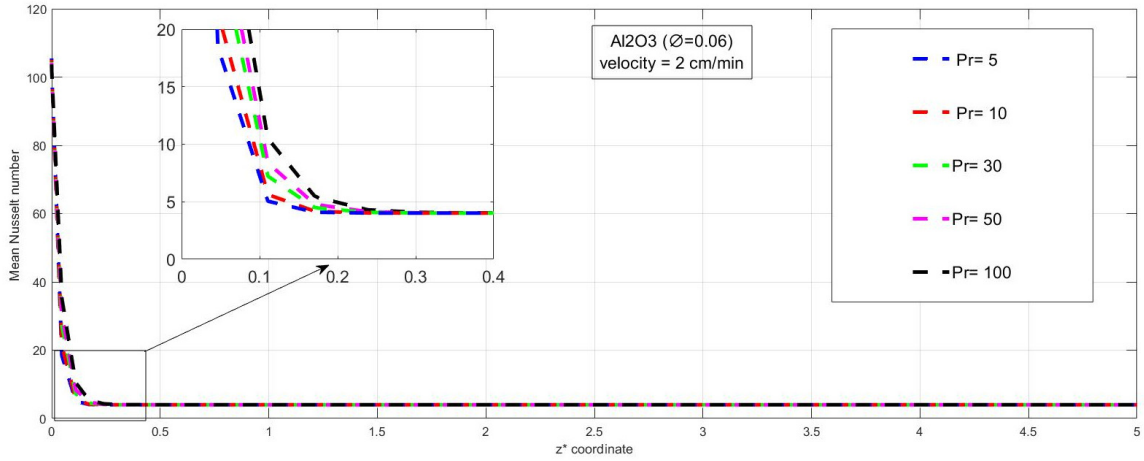

Figure 10. Mean Nusselt number along the conduit at different Prandtl number for Al_2O_3 nanofluid.

Figures 9 and 10 present the mean Nusselt number with different nanofluid velocities and Prandtl numbers. The sharp decreasing profile of the Nusselt number, that it starts with a high value then it faced a sharp sudden exponential decrease in the entrance region until it reached a constant value, which remains constant along the fully developed region. Noting that, friction factor and heat transfer coefficient stay constant in the fully developed region without any effect from the nanofluid velocity or the Prandtl number.

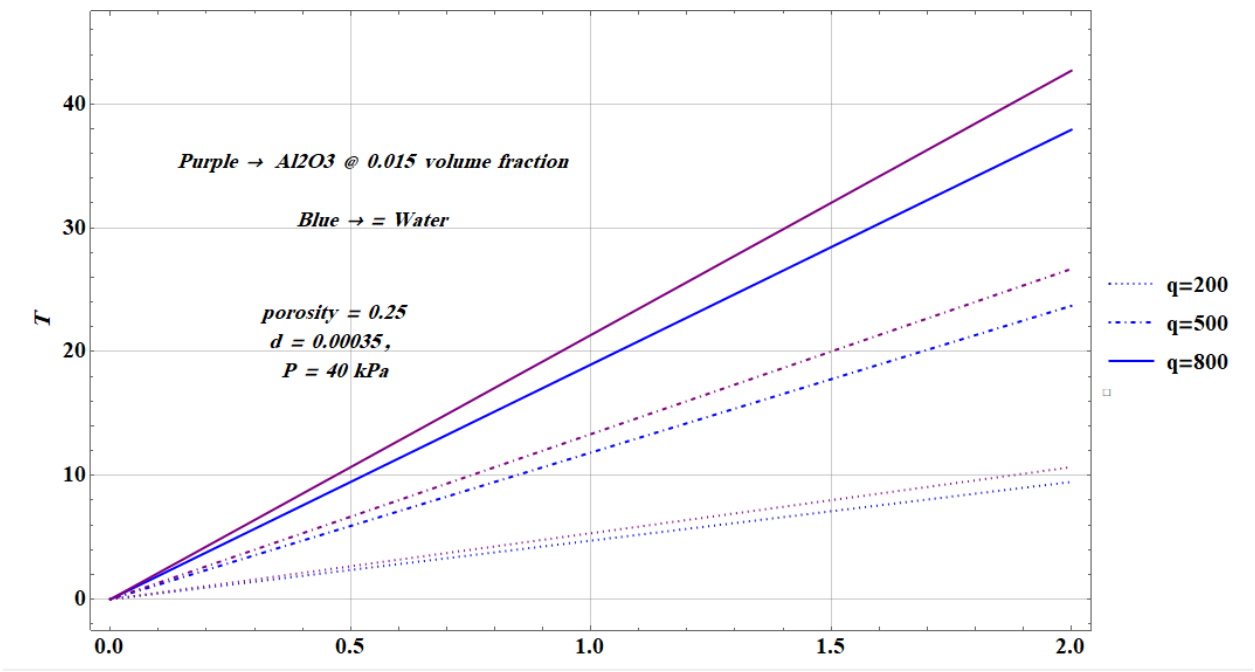

Figure 11. Temperature difference with Z coordinate at 1.5% volume fraction and different q for Al_2O_3 nanofluid compared with water.

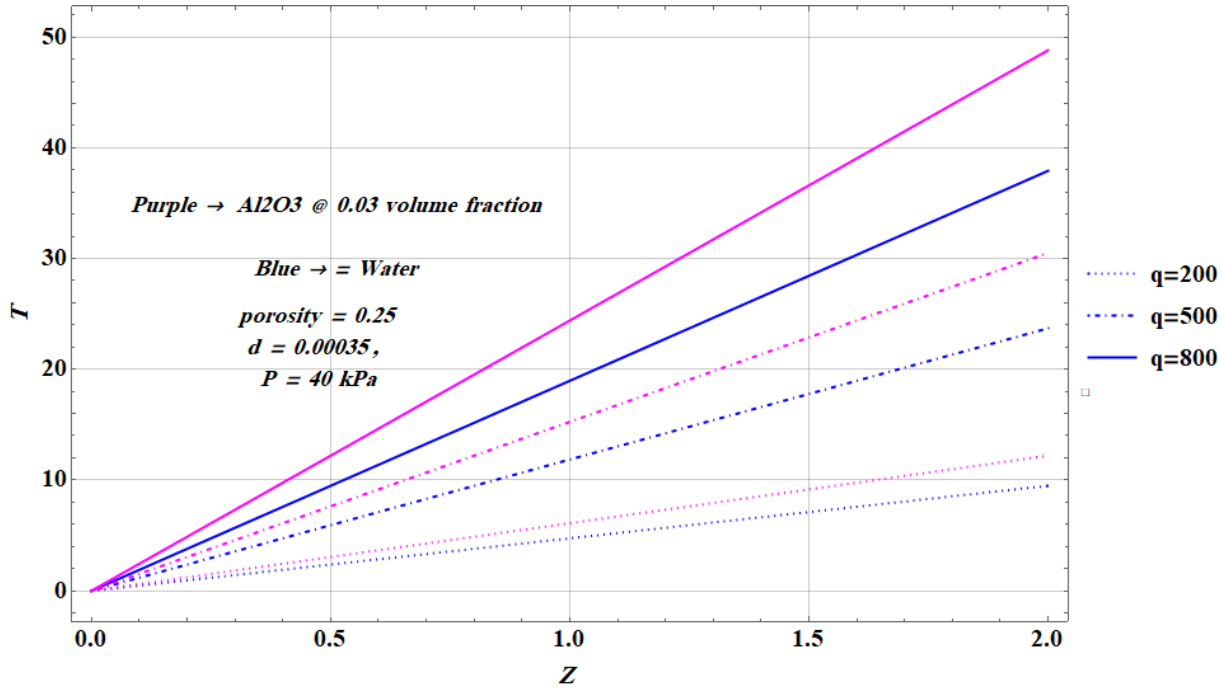

Figure 12. Temperature difference with Z coordinate at 3% volume fraction and different q for Al_2O_3 nanofluid compared with water.

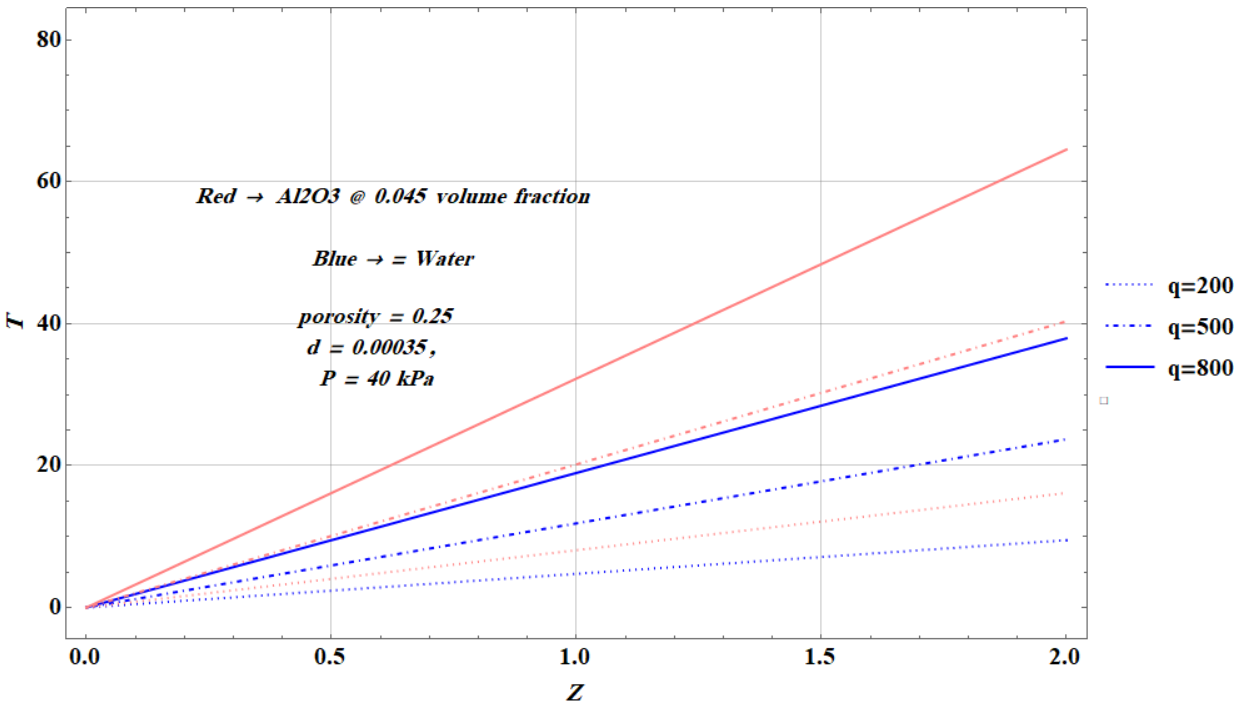

Figure 13. Temperature difference with Z coordinate at 4.5% volume fraction and different q for Al_2O_3 nanofluid compared with water.

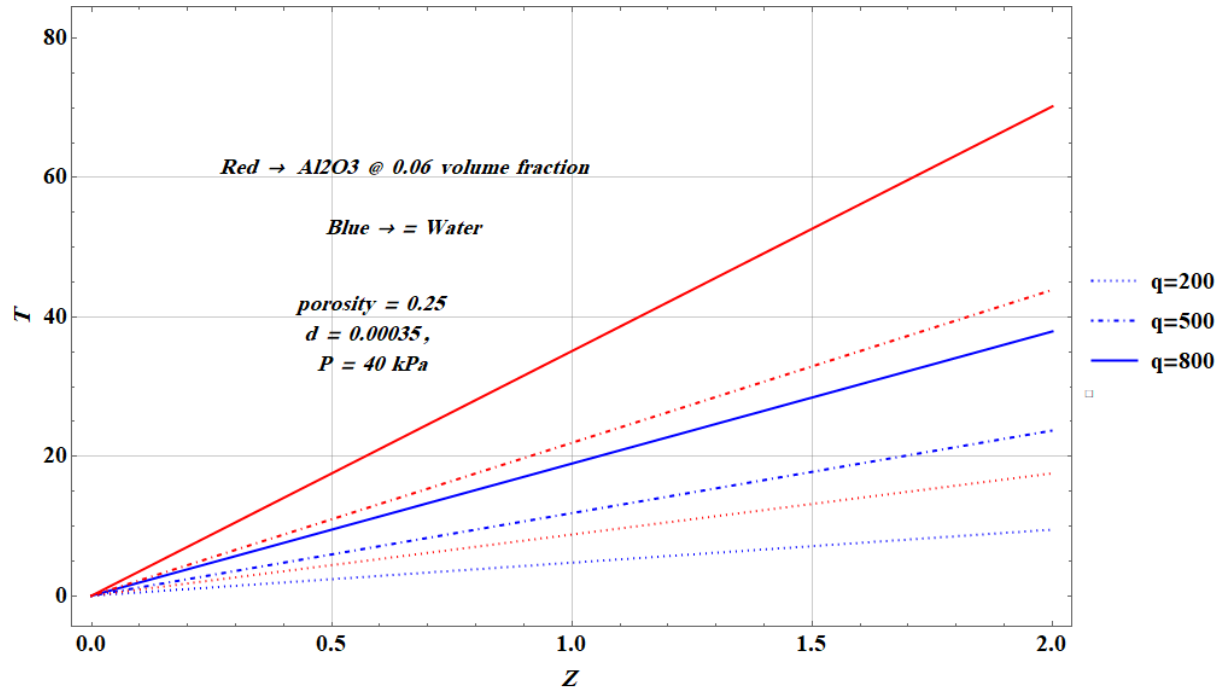

Figure 14. Temperature difference with Z coordinate at 6% volume fraction and different q for Al_2O_3 nanofluid compared with water.

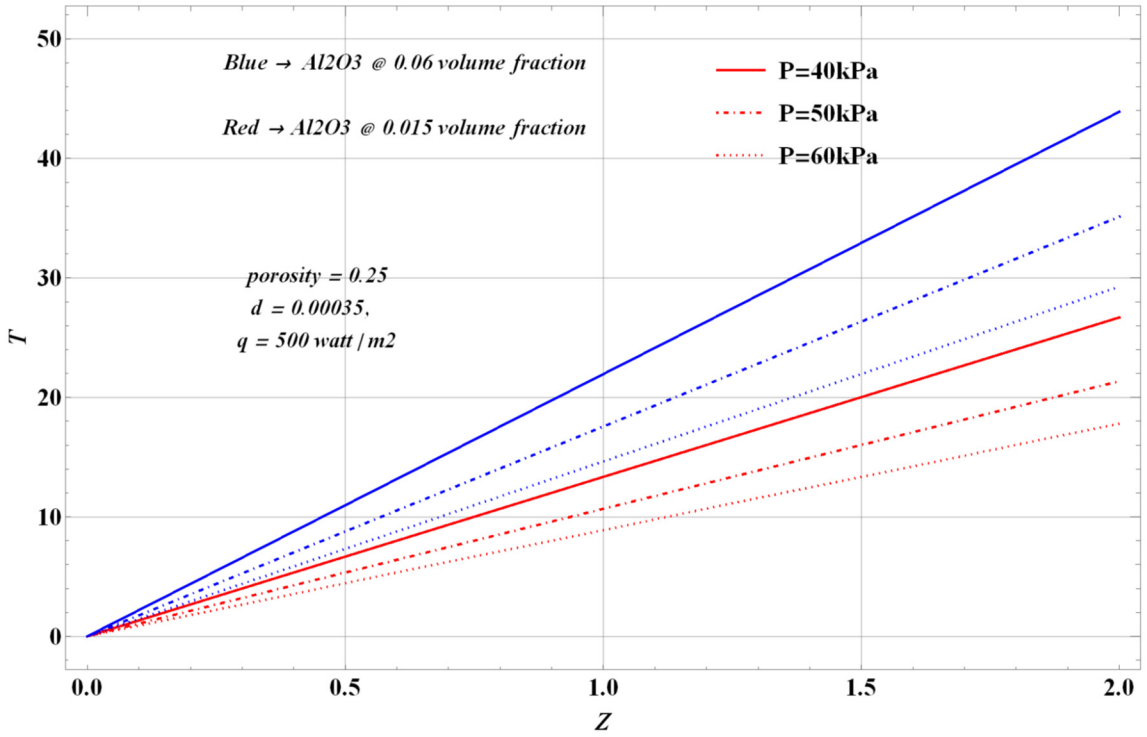

Figure 15. Temperature difference with Z coordinate at different volume fraction and pressure for Al_2O_3 nanofluid at 500 W/m^2.

In the fully developed region, Figures 11 to 14 show a comparison between nanofluid with different solid volume fractions and water. The mean temperature variation with axial coordinate for nanofluid and water at different heat flux are shown in the figures. The performance of the nanofluid is better than water at the same heat flux. It is concluded that the solid volume fraction of the nanoparticles in the nanofluid has a significant effect on the temperature variation, where the increase in the fraction lead for increase in the temperature variation.

Figures from 15 to 17 show the effect of pressure, pore diameter, porosity, and tube diameter at a constant heat flux (500 W/m^2) on the temperature variation along the tube.

Figure 15 presents how the temperature affected by the pressure at different φ for the nanofluid. It is noted that, as the pressure increase, the temperature decrease, that is because the increasing in pressure leads to increasing in the nanofluid velocity. Figure 16 shows the effect of porosity on temperature variation. The porosity has a significant inverse effect with the temperature, where the slight increase in porosity, lead for a significant decrease in the temperature variation.

Figure 17 shows the effect of solid particle diameters of the porous media on the temperature variation. The same effect as porosity, particle diameters has also a significant inverse effect with the temperature, where the slight increase in the particle diameter, lead for a significant decrease in the temperature variation.

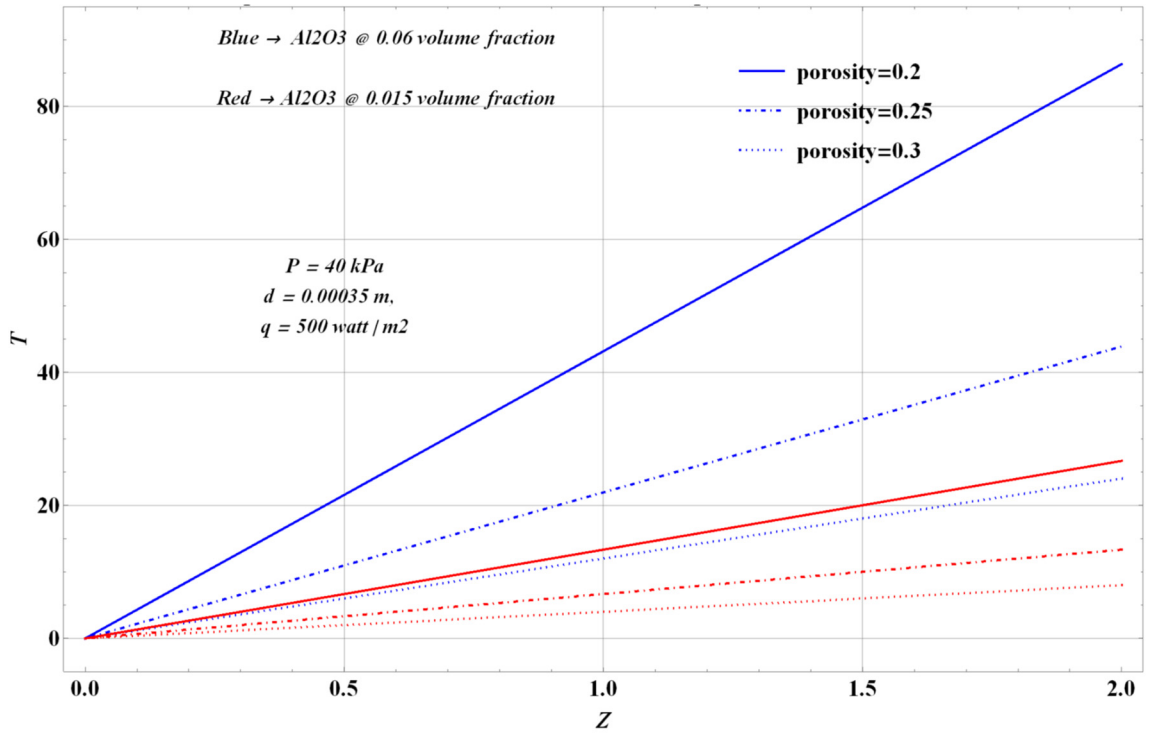

Figure 16. Temperature difference with Z coordinate at different volume fraction and porosity for Al_2O_3 nanofluid at 500 W/m^2.

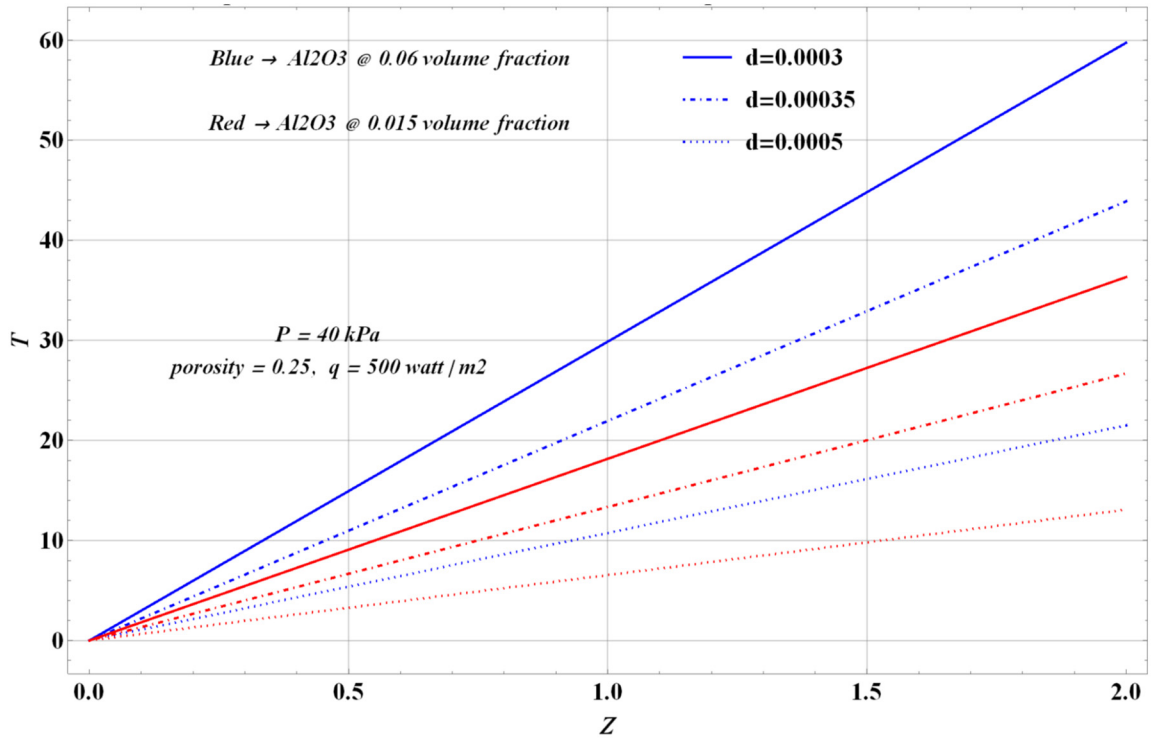

Figure 17. Temperature difference with Z coordinate at different volume fraction and particles for Al_2O_3 nanofluid diameter at 500 W/m^2.

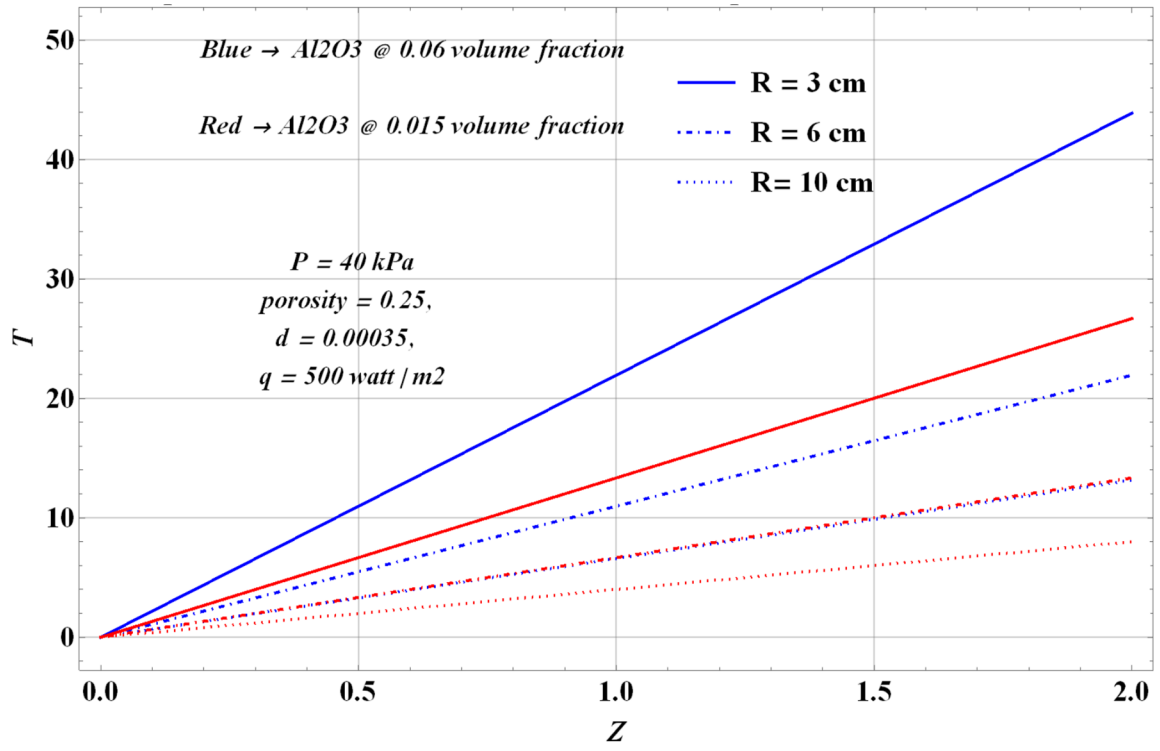

Figure 18. Temperature difference with Z coordinate at different volume fraction and tube radius (r) for Al_2O_3 nanofluid at 500 W/m^2.

The previous calculations were based on the tube radius of 3 cm, the effect of the tube radius is illustrated in Figure 18, the increase in the tube radius caused a decrease in the temperature variation as shown in the figure.

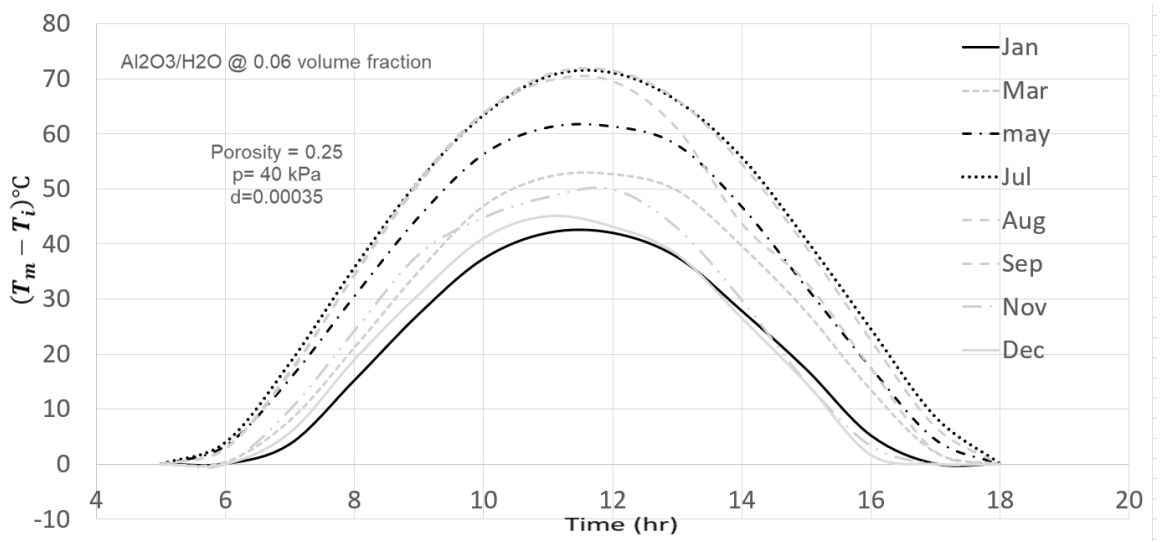

Figure 19. Temperature variation T(°C) during the day time(hr) at different heat flux for different months in Amman for Al_2O_3 with 6% solid volume fraction.

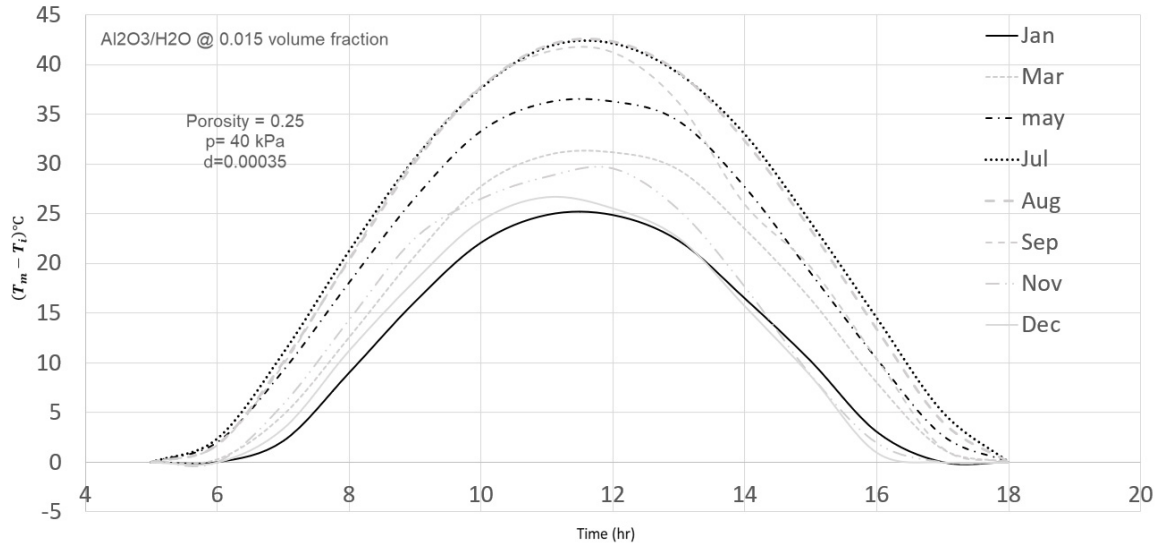

Figure 20. Temperature variation T(℃) during the day time(hr) at different heat flux for different months in Amman for Al_2O_3 with 1.5% solid volume fraction.

Figures 19 and 20 present the temperature variation at different heat fluxes in Amman for different ∅ for the nanofluid. The data of irradiances were taken from the from "Photovoltaic Geographical Information System" (PVGIS) and the temperature variation was calculated depending on that data. The high values of temperature were found in summer months, July and August. But the lowest were in the winter in December and January. Thus, due to the irradiance be maximum in summer and minimum in winter. The daily peak for the curve is different from month to month, that is due to the difference of solar noon between the months.

Figures 21 and 22 present the storage capacity in winter (January) and summer (August) at specified conditions and parameters shown on the figures. The conditions and the parameters can be changed to meet the required temperature. It is noted that the increase in the nanoparticles solid volume fraction will increase the temperature that can be achieved.

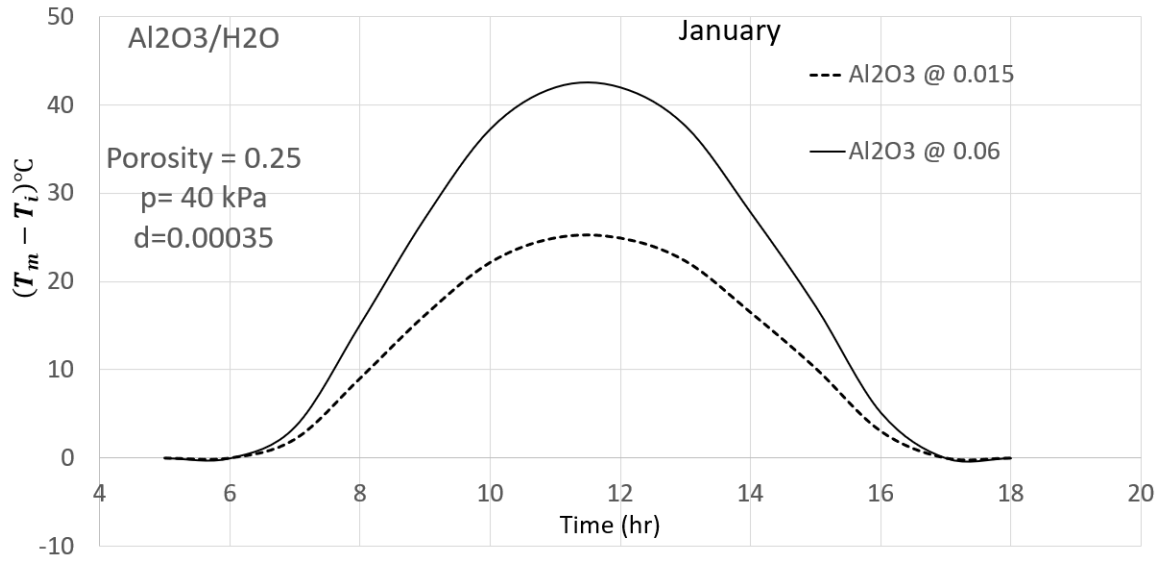

Figure 21. Temperature variation T(°C) during the day time(hr) in Amman for Al_2O_3 in January.

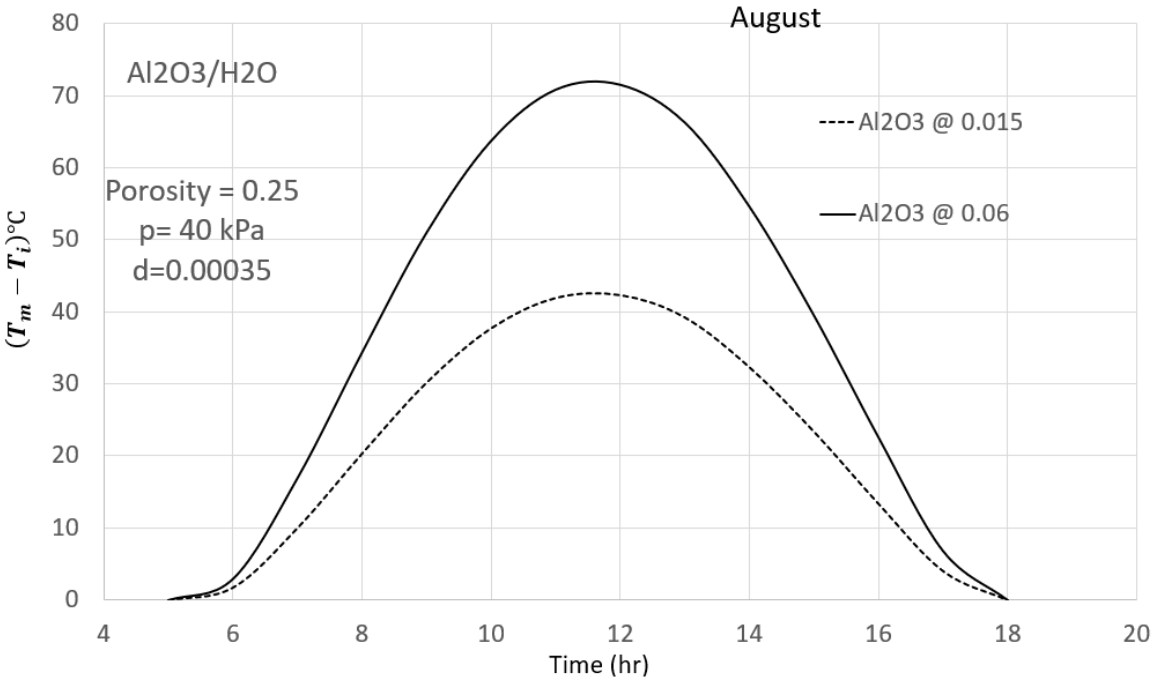

Figure 22. Temperature variation T(°C) during the day time(hr) in Amman for Al_2O_3 in August.

5. Conclusions

In the present work, a novel model of Al_2O_3 water-based nanofluid embedded in a saturated porous media was investigated theoretically. The governing equations were solved numerically in the entrance region using the finite difference method and analytically in the fully developed region. From the obtained results, it is concluded that:

i. The porous media enhance the performance of the energy storage since it has a high thermal conductivity.
ii. The use of nanofluid gave a better result than pure water in the presence of porous media, where the temperature difference for Al_2O_3 nanofluid with a solid volume fraction of 4.5% almost reached 40 ℃ with heat flux of 500 $Watt/m^2$, compared to a temperature difference around 25 ℃ when using water under the same conditions.
iii. The analysis of the behave of the Nusselt number shows that through the entrance region, it starts with a maximum high value, then it sharply decreases to reach a constant value. While the value of the Nusselt number remains constant in the fully developed region, and it is calculated and found to be equal to 4.
iv. The effect of different parameters as the heat flux, the porosity of the porous media, solid particle diameter of the porous media, nanoparticles volume fraction in the nanofluid, pressure, and tube diameter was investigated and studied.
v. It is found that the pressure, porosity, tube radius, and solid particles diameter of the porous media had an inverse relation with the temperature variation along the tube, where the increase of any them, holding the other parameters not changed, leads for a decrease in the temperature and the heat energy stored. On the other hand, the increase of heat flux, and the nanoparticles enhance the performance and increase the temperature and the stored energy.
vi. The results prove that increasing the nanoparticles solid volume fraction in the nanofluid will enhance the system's performance. For instance, 1.5% solid volume fraction for the nanofluid with heat flux of 500 $Watt/m^2$ gave a temperature difference around 26 ℃, while it was almost 45 ℃ when the solid volume fraction for the nanofluid was 6% under the same conditions.
vii. The best results were obtained at low velocities and Prandtl number, where the low velocity means low Reynolds number.
viii. The decrease in the Prandtl number and nanofluid velocity leads to a decrease in entrance length, and thus the fully developed region achieved faster.
ix. The results for a natural heat flux was illustrated by taking Amman in Jordan as an example; it is clear that the required temperature variation can be achieved through changing the conditions and parameters such as the pressure, nanoparticles solid volume fraction in the nanofluid, the porosity of the porous media, solid particles diameter of the porous media, and the tube radius.

As a future work, the following are suggested:

i. Study the effect of changing the porous media, base fluid, or nanoparticles material.
ii. Study the suggested model experimentally and compare the outcomes and the results with this work that is done theoretically.

Conflict of interest

The authors declare no conflict of interest.

References

1. Sabiha MA, Saidur R, Mekhilef S, et al. (2015) Progress and latest developments of evacuated tube solar collectors. *Renewable Sustainable Energy Rev* 51: 1038–1054.

2. Chopra K, Tyagi VV, Pandey AK, et al. (2018) Global advancement on experimental and thermal analysis of evacuated tube collector with and without heat pipe systems and possible applications. *Appl Energy* 228: 351–389.
3. Choi SUS (1995) Enhancing thermal conductivity of fluids with nanoparticles. *American Society of Mechanical Engineers, Fluids Eng Div* 231: 99–105.
4. Baqaie Saryazdi A, Talebi F, Armaghani T, et al. (2016) Numerical study of forced convection flow and heat transfer of a nanofluid flowing inside a straight circular pipe filled with a saturated porous medium. *Eur Phys J Plus* 131.
5. Kasaeian A, Daneshazarian R, Mahian O, et al. (2017) Nanofluid flow and heat transfer in porous media: a review of the latest developments. *Int J Heat Mass Transfer* 107: 778–791.
6. Gautam A, Saini RP (2020) A review on technical, applications and economic aspect of packed bed solar thermal energy storage system. *J Energy Storage* 27: 101046.
7. Nield, DA, Bejan A (2017) Convection in Porous Media. Available from: https://doi.org/10.1007/978-3-319-49562-0.
8. Mahmoudi Y, Hooman K, Vafai K (2019) Convective Heat Transfer in Porous Media.
9. Muhammad MJ, Muhammad IA, Sidik NAC, et al. (2016) Thermal performance enhancement of flat-plate and evacuated tube solar collectors using nanofluid: a review. *Int Commun Heat Mass Transfer* 76: 6–15.
10. Rashidi S, Esfahani JA, Rashidi A (2017) A review on the applications of porous materials in solar energy systems. *Renewable Sustainable Energy Rev* 73: 1198–1210.
11. Ahmed OK, Mohammed ZA (2017) Influence of porous media on the performance of hybrid PV/Thermal collector. *Renewable Energy* 112: 378–387.
12. Tajik Jamal-Abad M (2017) Experimental investigation on the effect of partially metal foam inside the absorber of parabolic trough solar collector. *Int J Eng* 30: 281–287.
13. AlMasa'deh HA, Duwairi HM. Modeling of Fluid Flow and Heat Transfer inside a Saturated Porous Conduit at Constant Surface Heat Flux. Available from: https://doi.org/10.18280/mmc_b.860309.
14. Saedodin SAHZS, Zamzamian SAH, Nimvari ME, et al. (2017) Performance evaluation of a flat-plate solar collector filled with porous metal foam: Experimental and numerical analysis. *Energy Convers Manage* 153: 278–287.
15. Esfe MH, Bahiraei M, Hajbarati H, et al. (2020) A comprehensive review on convective heat transfer of nanofluids in porous media: Energy-related and thermohydraulic characteristics. *Appl Therm Eng,* 115487.
16. Alihosseini S, Jafari A (2020) The effect of porous medium configuration on nanofluid heat transfer. *Appl Nanosci* 10: 895–906.
17. Esmaeili M, Karami M, Delfani S (2020) Performance enhancement of a direct absorption solar collector using copper oxide porous foam and nanofluid. *Int J Energy Res* 44: 5527–5544.
18. Tay NHS, Liu M, Belusko M, et al, (2017) Review on transportable phase change material in thermal energy storage systems. *Renewable Sustainable Energy Rev* 75: 264–277.
19. Liu L, Su D, Tang Y, et al. (2016) Thermal conductivity enhancement of phase change materials for thermal energy storage: A review. *Renewable Sustainable Energy Rev* 62: 305–317.
20. Lohrasbi S, Miry SZ, Gorji-Bandpy M, et al. (2017) Performance enhancement of finned heat pipe assisted latent heat thermal energy storage system in the presence of nano-enhanced H_2O as phase change material. *Int J Hydrogen Energy* 42: 6526–6546.

21. Bazri S, Badruddin IA, Naghavi MS, et al. (2019) An analytical and comparative study of the charging and discharging processes in a latent heat thermal storage tank for solar water heater system. *Sol Energy* 185: 424–438.
22. Naghavi MS, Ang BC, Rahmanian B, et al. (2020) On-demand dynamic performance of a thermal battery in tankless domestic solar water heating in the tropical region. *Appl Therm Eng* 167: 114790.
23. Mahdi RA, Mohammed HA, Munisamy KM, et al. (2015) Review of convection heat transfer and fluid flow in porous media with nanofluid. *Renewable Sustainable Energy Rev* 41: 715–734.
24. Khanafer K, Tavakkoli F, Vafai K, et al. (2015) A critical investigation of the anomalous behavior of molten salt-based nanofluids. *Int Commun Heat Mass Transfer* 69: 51–58.
25. Corcione M (2011) Empirical correlating equations for predicting the effective thermal conductivity and dynamic viscosity of nanofluids. *Energy Convers Manage* 52: 789–793.
26. Kandelousi MS (2014) KKL correlation for simulation of nanofluid flow and heat transfer in a permeable channel. *Phys Lett A* 378: 3331–3339.
27. Doerr M, Frommherz M (2002) Graphite (C) Classifications, Properties & Applications.
28. Sanchez-Coronado J, Chung DDL (2003) Thermomechanical behavior of a graphite foam. *Carbon* 41: 1175–1180.
29. Vafai K (2015) Handbook of porous media. Crc Press.
30. Karaipekli A, Biçer A, Sarı A, et al. (2017) Thermal characteristics of expanded perlite/paraffin composite phase change material with enhanced thermal conductivity using carbon nanotubes. *Energy Convers Manage* 134: 373–381.
31. Kim JH, Jeong E, Lee YS (2015) Preparation and characterization of graphite foams. *J Ind Eng Chem* 32: 21–33.
32. Bianco V, Manca O, Nardini S, et al. (2015) Heat Transfer Enhancement with Nanofluids.
33. Oosthuizen P, Naylor D (1999) Introduction to Convective Heat Transfer Analysis. WCB/McGrawHill.

AIMS Press